Published in final edited form as:
Prog Retin Eye Res. 2007 January ; 26(1): 38–56.

Retinotopic Organization of Primary Visual Cortex in Glaucoma: Comparing fMRI Measurements of Cortical Function with Visual Field Loss

Robert O. Duncan, **Pamela A. Sample**, **Robert N. Weinreb**, **Christopher Bowd**, and **Linda M. Zangwill**
Hamilton Glaucoma Center Department of Ophthalmology University of California, San Diego

Abstract

Primary open angle glaucoma (POAG) is a progressive optic neuropathy characterized by retinal ganglion cell loss. Experimental primate glaucoma indicates neuronal degeneration of the lateral geniculate nucleus (LGN) and activity changes in the visual cortex (V1). Neuronal degeneration has also been shown in a post-mortem human study of the optic nerve, LGN and visual cortex. Functional magnetic resonance imaging (fMRI), a non-invasive means of inferring function-specific neuronal activity, provides an opportunity to evaluate glaucomatous changes in neuronal activity throughout the visual pathway *in vivo*.

The purpose of this study is to demonstrate that the relationship between visual field loss in human POAG and the functional organization of V1 can be measured using novel fMRI analysis methods. Visual field defects were measured using standard automated perimetry (SAP). A retinotopic map of visual space was obtained for V1, and the retinotopy data was fit with a template. The template was used to project regions within the visual field onto a flattened representation of V1. Viewing through the glaucomatous vs. fellow eye was compared by alternately presenting each eye with a scotoma-mapping stimulus. The resulting blood oxygen level dependent (BOLD) fMRI response was compared to interocular differences in thresholds for corresponding regions of the visual field.

The spatial pattern of activity observed in the flattened representation agreed with the pattern of visual field loss. Furthermore, the amplitude of the BOLD response was correlated on a pointwise basis with the difference in sensitivity thresholds between the glaucomatous and fellow eyes ($r = 0.53$, $p < 0.0001$).

The BOLD signal in human V1 is altered for POAG patients in a manner consistent with the loss of visual function. FMRI of visual brain areas is a potential means for quantifying glaucomatous changes in neuronal activity. This should enhance our understanding of glaucoma, and could lead to new diagnostic techniques and therapies.

Send correspondence to: Robert O. Duncan, Ph.D., Hamilton Glaucoma Center, Department of Ophthalmology, University of California, San Diego, 9415 Campus Point Dr., La Jolla, CA 92093-0946, Tel: (619) 302-2931, E-mail: rduncan@eyecenter.ucsd.edu
Commercial relationships:
R.O. Duncan, CR: R Heidelberg Engineering; P.A. Sample, CR: F Carl Zeiss Meditec, Welch-Allyn, Haag Streit; R.N. Weinreb, CR: F, R Carl Zeiss Meditec, R Heidelberg Engineering; C. Bowd, CR: none; L.M. Zangwill, CR: F Carl Zeiss Meditec, F and R Heidelberg Engineering.

1. Glaucomatous neuronal degeneration in the central nervous system

Glaucoma is a group of progressive optic neuropathies that share a common feature, a gradual loss of retinal ganglion cells accompanied by a progressive degeneration of the optic nerve. Left untreated, glaucoma results in irreversible vision loss or blindness. Glaucoma is the second leading cause of blindness worldwide, and will affect 79.6 million people worldwide (Quigley and Broman, 2006).

While intraocular pressure is a leading risk factor for glaucoma, the pathophysiology of neuronal degeneration in glaucoma is unknown. Primary open angle glaucoma (POAG) often causes vision loss in subjects with normal intraocular pressure, demonstrating that there are additional factors contributing to the disease (Weinreb and Khaw, 2004).

In addition to damaging retinal ganglion cells, POAG also damages post-retinal mechanisms, including the lateral geniculate nucleus of the thalamus (LGN) and the primary visual cortex (V1). Experimental primate glaucoma indicates neuronal degeneration of the LGN and activity changes in the visual cortex (Vickers et al., 1997;Crawford et al., 2000;Weber et al., 2000;Yucel et al., 2000;Crawford et al., 2001;Yucel et al., 2001,2003). Human LGN changes in glaucoma have been described (Chaturvedi et al., 1993), but the reported cell counts did not take changes in LGN volume into account (Weinreb et al., 1994). Neuronal degeneration has also been shown in a post-mortem human study of optic nerve, LGN and visual cortex (Gupta et al., 2006). POAG can affect several structures along the visual pathway before behavioral deficits are noticed. For example, by the time visual field defects are detected using perimetry, 50-60% of the ganglion cells may already be dead (Harwerth et al., 1999;Harwerth and Quigley, 2006). Structural changes in the retina and optic nerve head observed during ophthalmologic examination may also be detected before functional changes (Sommer et al., 1991;Johnson et al., 2003).

A greater knowledge of post-retinal mechanisms in POAG might provide clinicians with better tools for diagnosis and treatment. Animal models of glaucoma are informative, but the experimental glaucomas may stem from different pathologies than POAG. Experimental non-human animals primates are typically young, and glaucomatous progression occurs more rapidly in experimentally induced glaucoma relative to that in human POAG. Additionally, the experimental glaucomas are primarily caused by elevated intraocular pressure. For these reasons, human studies are preferred for understanding human disease. However, human histology studies have required post-mortem analysis, and thus disease-related changes cannot be monitored over time. Functional magnetic resonance imaging (fMRI), on the other hand, is a non-invasive means of inferring neuronal activity that can measure brain function over time *in vivo*. To date, only one fMRI study has investigated the effects of optic neuropathy on the occipital cortex of humans, and the techniques used were not optimal (Miki et al., 1996). Unfortunately, the methodology used in that study resulted in poor response localization, and neuronal and behavioral responses were not compared. A precise method for comparing visual field thresholds to activity in visual cortex is still needed. In the current study, novel fMRI techniques for measuring neuronal activity in the central nervous system of glaucoma patients have been presented. Unlike previous fMRI studies of optic neuropathy, this approach can accurately localize the representation of visual scotomas within the flattened representation of V1. The improved methodology will make it easier to compare glaucomatous changes in neuronal activity measured from human V1 to changes in visual field thresholds, thus providing clinically relevant information that may lead to new diagnostic techniques and therapies.

2. Retinotopic mapping in humans using fMRI

FMRI has rapidly become the standard for inferring neuronal activity in human subjects because (1) it is non-invasive, (2) it has reliable response localization, and (3) it has superior

spatial resolution compared to previously developed technologies like positron emission tomography (PET). To acquaint the non-specialist, the basics of fMRI will be briefly reviewed as they relate to the study of visual function in glaucoma.

Increases in neuronal activity are accompanied by changes in blood oxygenation that give rise to changes in the MR signal. This Blood Oxygenation Level Dependent (BOLD) signal serves as the basis for a majority of studies that measure brain function *in vivo*. Changes in blood oxygenation were originally found to affect the MR signal in rat during experiments where the oxygen content of inspired air was manipulated (Ogawa et al., 1990). Soon thereafter, several studies utilized the BOLD effect for functional brain mapping in humans (Bandettini et al., 1992;Frahm et al., 1992;Ogawa et al., 1992), including the first study of visually evoked BOLD responses (Kwong et al., 1992). The BOLD effect occurs for two reasons (Buxton, 2002). First, local concentrations of deoxyhemoglobin generate magnetic field gradients along the blood vessels that reduces the MR signal. Second, increases in neuronal activity result in decreases in the local oxygen extraction fraction in the blood that, in turn, causes a corresponding drop in the local concentration of deoxyhemoglobin. The net reduction of deoxyhemoglobin during brain activity manifests in an increase in the MR signal.

BOLD fMRI is the preferred method for retinotopy, which is the process of determining the correspondence between a visually selective neuron and its receptive field in visual space. In the case of the V1, mapping the representation of visual space is straightforward because the cortical topography is such that adjacent regions along the cortical surface correspond to adjacent regions in visual space. Even though the first visual fMRI experiment did not attempt retinotopic mapping (Kwong et al., 1992), another early experiment mapped the visually evoked fMRI response along a cortical ribbon with four topologically distinct regions (Schneider et al., 1993). Refined retinotopic mapping was not possible until Engel and colleagues (Engel et al., 1994) developed phase-encoded retinal stimulation. In their experiment, an annular contrast-reversing (8 Hz) checkerboard pattern was presented at the center of gaze (Figure 1A). This ring expanded in size until the beginning of the next cycle, when the stimulus returned to its original size and the period of expansion repeated. Expanding rings elicit a traveling wave of activity in V1 that is phase-locked with the period of the stimulus. As a result of phase encoding, Engel and colleagues could distinguish between the cortical representation of the fovea and that of the periphery.

However, the notion of retinotopic mapping did not fully mature until Visual Field Sign (VFS) mapping was developed (Sereno et al., 1995). VFS mapping is typically used to define the borders of V1, V2, V3, V3a and hV4 on a computationally flattened representation of the cortical surface (Dale and Sereno, 1993). In addition to the expanding ring, VFS mapping employs a rotating wedge stimulus, which is composed of a contrast-reversing checkerboard pattern that revolves clockwise around a fixation target for several cycles (Figure 1B). The borders of visual areas can be distinguished by reversals in the sign of the phase of the fMRI response to the rotating wedge. While the size and location of visual areas can vary greatly between individuals (DeYoe et al., 1996), experiments using VFS mapping have determined that fMRI responses to visual stimuli are spatially invariant within 1.1 mm of cortex (Engel et al., 1997).

VFS mapping methods are not particularly suited for glaucoma research. Glaucoma patients typically have localized visual field defects. To measure the extent/existence of glaucomatous changes in neuronal activity in V1, the borders of these defects must be mapped on the cortical surface as a region of interest (ROI). However, the sluggish hemodynamic response creates a delay between the instance of visual stimulation for phase-encoded stimuli and the BOLD response, and thus it is difficult to precisely determine which region of V1 corresponds to the scotoma. One possible solution to this problem would be to map the visual field using static

stimuli presented throughout the visual field. However, this process is too time-consuming and expensive to be practical. Furthermore, hemodynamic responses to small visual stimuli are spatially blurred, making it difficult to localize the borders of the ROI representing the scotoma.

One alternative to VFS mapping is based on a template-fitting approach (Duncan and Boynton, 2003). Static stimuli are first used to map landmarks in V1. Then, templates are fit to the resulting activity. Finally, the templates are used to project the borders of the scotoma onto the flattened cortical surface as a ROI. The technique takes advantage of the fact that there is a logarithmic relationship between each hemifield of visual space and its corresponding cortical representation in V1 (Schwartz, 1980). Template fitting is superior to VFS mapping because static stimuli do not introduce the temporal delay that is inherent to phase-encoded stimuli. Moreover, ROIs can be defined robustly for sub-regions of V1 that do not receive direct retinal input.

3. Prior investigations of cortical activity in human glaucoma

A number of studies have demonstrated an ability to detect glaucomatous damage using multifocal visual evoked potentials (mfVEP) (Klistorner et al., 1998;Graham et al., 2000;Hood et al., 2000;Hasegawa et al., 2001;Goldberg et al., 2002;Hood and Greenstein, 2003;Thienprasiddhi et al., 2003;Hood et al., 2004;Graham et al., 2005), positron emission tomography (PET) (Kiyosawa et al., 1989), and single photon emission computed tomography (SPECT) (Sugiyama et al., 2006;Yoshida et al., 2006). Each technique has its limitations. Although mfVEP has been used successfully to objectively measure neural activity *in vivo*, the technique is restricted by the fact that signals cannot be accurately localized to specific brain regions (Fortune and Hood, 2003). Furthermore, because the effective spatial resolution of mfVEP is approximate 7° in the periphery, relatively small peripheral scotomas might not be detected (Hood and Greenstein, 2003). PET and SPECT are not practical for repeatedly monitoring glaucomatous progression because they require radioisotopes. Ultimately, the spatial resolution of these techniques limits their ability to compare cortical activity with measurements of visual function in a retinotopic manner.

The spatial resolution of fMRI affords the opportunity to scrutinize restricted regions of cortex, enabling comparisons of diseased and fellow tissue receiving input from the same eye. Only one other fMRI study of optic neuropathy compared visual field defects to fMRI responses in V1 (Miki et al., 1996). In that report, a heterogeneous population of optic neuropathies was studied in patients ranging from 19 to 70 years of age using traditional retinotopic techniques and found that there was a general correspondence between the pattern of visual field defect and the pattern of the fMRI response. Pathologies included traumatic optic neuropathy, compressive optic neuropathy, developmental glaucoma, capsular glaucoma, secondary open-angle glaucoma, and optic atrophy cause by sellar tuberculoma or pituitary adenoma. As a consequence, it is difficult to generalize to POAG. In addition, the investigators did not make quantitative comparisons between visual fields and brain responses.

Traditional MRI methods (e.g., T1-weighted imaging) can already be used to measure the volume of anatomically distinct visual areas like the LGN (Brodsky et al., 1993;Fujita et al., 2001). However, fMRI has two key advantages over traditional MRI for measuring glaucomatous changes in neuronal activity. First, fMRI can measure degeneration from visual areas that can only be defined using functional criteria, which is important considering the variability of visual areas between individuals (Duncan and Boynton, 2003). Second, fMRI can measure functional activity related to specific visual pathways (Kleinschmidt et al., 1996;Demb et al., 1998;Wandell et al., 1999;Bedwell et al., 2004;Schneider et al., 2004;Liu and Wandell, 2005). For example, anatomical MRI methods can measure the total volume of LGN, but only fMRI can distinguish between the functional activity associated with specific

visual pathways (Schneider et al., 2004). Recent developments in fMRI analysis allow for the computational projection of visual scotomas onto the flattened representation of V1 (Duncan and Boynton, 2003). These analysis tools were incorporated in the following study, which was designed to quantify the correlation between fMRI responses and several visual function tests on a much finer spatial scale than studies using other brain imaging analysis techniques. Future fMRI studies will quantify glaucomatous changes in the central nervous system and function-specific neuronal activity associated with the three primary visual pathways.

4. Comparing fMRI responses to visual function in glaucoma

4.1. Methods

4.1.1. Subjects—Six asymmetric POAG patients with one glaucomatous eye and a less affected "fellow" eye were included. All patients presented with abnormal visual field results and glaucomatous appearance of the optic disk based on stereophoto review in at least one eye. Abnormal visual fields were defined as a repeatable defect in at least two consecutive visits. Glaucomatous optic disks were defined as having either asymmetric vertical cup-to-disk ratio > 0.2, rim thinning, notching, excavation, disk hemorrhages, or nerve fiber layer defects based on masked analysis of stereoscopic photographs and consensus of two reviewers. Visual fields were judged on the number of pattern deviation points (PD) that were significantly different from the normative database at $p < 0.05$ or worse. Patient fellow eyes had markedly fewer visual field abnormalities relative to the glaucomatous eye (χ^2, $p < 0.0001$). Patients were evaluated at the Hamilton Glaucoma Center at the University of California San Diego (UCSD) between July of 2004 and August of 2005. The patients in this cross-sectional study were recruited from a longitudinal study designed to evaluate the optic nerve structure and visual function in glaucoma (Diagnostic Innovations in Glaucoma Study - DIGS). A summary of relevant patient data appears in Table 1.

4.1.2. Criteria for inclusion and exclusion—All patients underwent complete ophthalmologic examination including slitlamp biomicroscopy, intraocular pressure measurement, dilated stereoscopic fundus examination, and stereophotography of the optic nerve heads. Good quality simultaneous stereoscopic photographs were obtained for all patients.

Informed consent was obtained from all patients after the nature and possible consequences of the study were explained, and the UCSD Internal Review Board approved all methods pertaining to the use of human subjects. The study adhered to the declaration of Helsinki for research involving human subjects.

A neuroradiologist, reviewed the anatomical reference volumes and found no evidence of non-glaucomatous pathology that could present as glaucoma. Patients were also screened for standard MRI exclusion criteria: no conditions/medications known to affect cerebral metabolism, no metal in the body that could not be removed, and no history of claustrophobia.

4.1.3. Visual function testing—Standard automated perimetry (SAP) was conducted in each patient using the 24-2 Swedish Interactive Threshold Algorithm (SITA) (Carl Zeiss Meditec Inc., Dublin, CA) of the Humphrey Visual Field Analyzer (HFA). The program uses 52 test locations presented in a six-degree grid, and stimuli are generated using conventional parameters (Goldmann size III stimulus, 10 cd/m^2 white background). An optimal lens correction was placed before the tested eye, and the fellow eye was occluded with an eye patch. Exclusion criteria for visual fields included unreliable visual fields (defined as fixation loss, false negative, and false positive errors $\geq 25\%$, unless false negatives could be explained by significant field loss). All patients in this study had five or more standard visual fields. Results were compared to the HFA normative database.

4.1.4. Evaluation of stereophotographs—Evaluation of glaucomatous structural damage to the optic disk was based on assessment of simultaneous stereoscopic optic disk photographs (Nidek Stereo Camera Model 3-DX, Nidek Inc, Palo Alto, CA). Two experienced graders evaluated the photographs, and each grader was masked to the patient's identity, the other test results, and the other grade. Discrepancies between the two graders were resolved either by consensus or by adjudication by a third experienced grader.

4.1.5. General fMRI methodology—BOLD fMRI was used to infer neuronal activity in the contralateral hemisphere of these patients. FMRI images were acquired at the Center for Functional Magnetic Resonance Imaging at UCSD using a General Electric 3.0 Tesla HD Signa Excite scanner with an 8-channel brain coil. Visual stimuli were presented through a pair of fiber optic Silent Vision goggles (Avotec Inc., Stuart, FL). The general specifications of the visual presentation system follow: field of view = 30H × 23V degrees; focus +/− 6 D; maximum luminance = 28.9 cd/m^2; resolution = 1024H × 768V, 60 Hz refresh rate. Visual stimuli were generated using the Psychophysics Toolbox (Brainard, 1997;Pelli, 1997) for Matlab (Mathworks, Natick, MA) on a PowerBook G4 computer (Apple, Cupertino, CA).

Each patient participated in up to three one-hour scanning sessions that included both functional and anatomical scans. A high-resolution anatomical scan was obtained using a standard T1-weighted gradient echo pulse sequence (FSPGR, 1×1×1 mm resolution). This anatomical scan provided a reference volume anatomy for each patient. Up to eight functional scans were acquired from each patient during each session. For each functional scan, 130 temporal frames were acquired using a low-bandwidth echo planar imaging (EPI) pulse sequence lasting 260 s (TR = 2 s, TE = 30 ms, flip angle = 90°, 24 coronal slices of 3 mm thickness and 3×3 mm resolution, FOV = 20 cm). The first ten temporal frames (20 s) were discarded to avoid magnetic saturation effects. Scanning sessions ended with an anatomical scan that was used to align functional data across sessions to a patient's reference volume. Cortical flattening techniques and methods for projecting functional data onto the flattened representation have been described in detail elsewhere (Duncan and Boynton, 2003). The occipital pole was flattened initially, and V1 was re-flattened after the borders of visual areas (V1, V2, V3) were defined using traditional retinotopy (Sereno et al., 1995).

4.1.6. FMRI stimuli—In the first scanning session, standard binocular stimuli were used to project the visual world onto a flattened representation of the cortex in retinotopic coordinates. During a given scan, patients viewed either an expanding ring (Figure 1A) or a rotating wedge (Figure 1B) made from a contrast-reversing black and white checkerboard pattern (100% contrast; 8 Hz flicker). Stimuli were presented at the center of the screen on a mean gray background, and patients fixated on a target (0.25° × 0.25°) at the center of the screen. The width of the expanding rings was roughly 1/6 of the eccentricity, and the polar angle of the wedges was 45°. The rings expanded at 0.2°/sec and the rotating wedges moved at an angular velocity of 9°/sec. Expanding rings and rotating wedges were presented for 6 and 1/2 cycles of 40 s each. Data from the first 1/2 cycle was discarded to avoid magnetic saturation effects. In addition to the rings and wedges, the horizontal and vertical meridians were mapped using alternating "hourglass" and "bow tie" shaped checkerboard patterns (Figures 1C and D respectively). Each square was 1×1° of visual angle. Meridian-mapping stimuli were composed of two mirror-symmetric, triangular regions spanning 90° of polar angle about the meridian. During a given scan, the two meridian-mapping stimuli were alternated every 20 s for 6 and 1/2 40 s cycles (including the discarded 1/2 cycle). Each of three retinotopy stimuli was repeated twice for a total of six functional scans during the first session. The stimulus period (20 sec on/off) and the temporal frequency of the contrast-reversing checkerboard (8 Hz) were selected from values known to elicit a maximum BOLD response from V1 (DeYoe et al., 1994;Engel et al., 1994;Sereno et al., 1995;Engel et al., 1997;Tootell et al., 1998).

Visual areas in occipital cortex (V1, V2, V3, V3a, and hV4) represent either one quadrant or one hemifield of visual space. Thus, the meridian-mapping stimulus evokes a pattern of BOLD activity in the flattened cortical representation that defines the borders of these visual areas. Additionally, BOLD responses to the rotating wedge reverse temporal phase at the borders of these visual areas. The borders of visual areas were defined by the experimenter based on the pattern of BOLD activity to these stimuli.

In the second scanning session, the cortical representation of a 16° isopter in the affected left or right visual hemifield was measured. Binocular stimuli were made from contrast-reversing arcs that extended through the superior and inferior quadrants of the glaucomatous visual field (Figures 1E and F respectively). Arcs were composed of contrast-reversing checkerboard patterns with a radius of 16° of visual angle and a width of 2.7° (determined as the average of outer and inner radii). Each square subtended 7.5° of polar angle. Patients were instructed to fixate on a target (0.25° × 0.25°) positioned at one corner of the screen while one arc was presented in the periphery. For each scan, one arc was presented alternately with a period of no stimulation (mean gray screen) every 1/2 cycle (20 s). Four scans were conducted measuring responses to the 16° arc in both the superior and inferior quadrants, yielding a total of 8 scans. Responses to the two arcs were projected onto the flattened representation of V1, and the responses were averaged to obtain the representation of the 16° isopter for the hemifield of interest.

In the third scanning session, patients fixated a target in one corner of the screen while a “full-field” contrast-reversing checkerboard pattern was presented to the quadrant of visual space with the most visual loss (Figure 1G). Each square spanned 1×1° of visual angle. However, unlike sessions one and two, where all viewing was binocular, patients viewed this scotoma-mapping stimulus monocularly through their right or left eye in alternating epochs of 20 s (equivalent to one half-cycle). The shape of the fixation target served to direct patients as to which eye should be open. Patients controlled monocular viewing by winking. Non-compliance could potentially introduce random noise in the fMRI responses to the stimuli. Such noise, however, would not seriously affect the results unless the patient opened the incorrect eye perfectly out of phase with the stimulus. To insure patient compliance, the experimenter monitored the patient’s eye movements via an infrared camera installed in the video presentation system. Eye position was recorded using iView dark-pupil eye tracking software (SMI, Teltow, Germany). Eye traces were processed in accordance to protocols developed previously (Krauzlis and Miles, 1996). Velocity and acceleration were computed by applying a 29-point finite impulse response (FIR) filter (−3dB at 54Hz). Acceleration and velocity thresholds were used to identify the onset of saccades and eye blinks. Deviations in eye position beyond a certain distance (3 deg) were labeled as “breaks of fixation” and their position was recorded. There was no change in the stimulus presentation if there was a break in fixation. The total number of fixation breaks was determined, and chi-squared tests were used to determine if there was a difference associated with different monocular viewing conditions or, if the number of eye movements varied between the four quadrants of visual space. These analyses revealed that the direction of fixation breaks was spatially distributed and not associated with viewing through the glaucomatous or fellow eye (χ^2, all $p > 0.10$). Furthermore, the number of fixation breaks did not differ between glaucoma and control subjects (χ^2, $p > 0.10$). Thus, patients were able to fixate well. Patients fully closed each eye according to directions in the third session, where monocular viewing alternated between eyes.

4.1.7. Projecting patterns of visual field loss onto the cortex—The SAP visual fields for both eyes of each patient are presented in Figure 2. For each glaucomatous eye, corresponding visual fields for SAP were scrutinized, and the quadrant with the most damage was selected based on the number of test locations that deviated statistically from the normative database. The area of the visual field with the most extensive loss was manually defined

(locations with PD greater than 95% confidence limits). The integrity of the scotoma was verified for each patient by looking at visual fields obtained during prior or subsequent research visits.

Responses to the retinotopy stimuli were fit with templates, which were then used to project visual scotomas onto the flattened representation of cortex. The fMRI responses from the first and second scanning sessions were fit using conformal mapping techniques to obtain a template for each patient (Duncan and Boynton, 2003). Templates were then used to project the portion of the visual field with the most extensive loss (Figure 3A, red line), onto the flattened representation of V1 (Figure 3D, black line). The projected ROI was later used to restrict the analysis to cortical regions corresponding to regions of visual space with most extensive loss.

The template fitting technique was originally developed to compare cortical magnification to spatial acuity thresholds in normal observers (Duncan and Boynton, 2003). In that study, the template fitting technique was sensitive enough to find a within-subject correlation between spatial acuity at any location in the visual field and the size of the corresponding cortical representation in cortex. Here, the technique was modified slightly for scotoma mapping in glaucoma patients. Templates were derived from a conformal mapping method developed by Schwartz (Schwartz, 1980). In this approach, two-dimensional visual space is projected onto the two-dimensional flattened cortex using the formula $w = k \times \log(z+a)$, where z is a complex number representing a point in visual space, and w represents the corresponding point on the flattened cortex. The parameter a represents the proportion of V1 devoted to the foveal representation, and the parameter k is an overall scaling factor. An additional parameter, b, was added to scale the width of the map. To achieve this, the real and imaginary components of the projected positions, w, were separated and the real component was scaled by parameter b. This modification affords better fits by sacrificing the preservation of local isotropy. The templates in this study were composed of four components representing the 16° isopter, the horizontal meridian, the superior vertical meridian, and the inferior vertical meridian (Figure 3). Six parameters describe the template; the overall size (k), the position (dx, dy), the rotation (da), the foveal representation (a), and the width (b).

Templates were fit to the fMRI activity map by adjusting the parameters to maximize the image intensity (i.e., the line-integral) under the projected curves. Parameter values from the best-fitting template were obtained using a nonlinear optimization technique in Matlab. First, straight lines that roughly fit fMRI responses to the superior and inferior vertical meridians were superimposed onto the retinotopy data (Figure 3B, yellow lines). Second, the intersection of these lines was computed and that point was designated as the fovea (Figure 3B, red dot). Third, a point corresponding to the peak activity for the horizontal meridian-mapping stimulus was selected (Figure 3B, blue dot). Then, the software automatically generated a generic template that was rotated and shifted to fit the data based on the parameters selected (Figure 3C). All the other parameters in the template (a, b, and k) were set to default values that roughly corresponded to the average V1 size (775 mm^2), which was determined by averaging the area from 10 healthy control subjects in a previous experiment (Duncan and Boynton, 2003). Note that varying the size of the initial template does not have an affect on the final fit (Duncan and Boynton, 2003). The template was then fit to the data using a two-stage optimization routine (Figure 4). In the first stage, each individual model parameter was optimized to fit the template to all activity maps simultaneously. In the second stage, the best-fitting template was generated by simultaneously fitting all parameters to the activity maps. Note that the parameter for the overall size of the template, k, was excluded from the final optimization because, without a constraint on the size of the template, the fit would converge to the trivial condition of a single point over a location of maximum amplitude.

The optimized fits for the patient 6 in Figure 2 are superimposed upon the grayscale activity maps in Figure 4. The colored lined superimposed upon the patterns of activity show the locations, projected using parameters from the best-fitting template, of the 16° isopter and meridian-mapping stimuli. Each component is color coded to match the scheme outlined in the inset. Figure 4A displays fits to the 16° isopter stimuli, and Figures 6B-D display fits to the meridian-mapping stimulus. Figure 4E shows the best-fitting template for all stimuli superimposed upon the responses to the meridian-mapping stimulus.

Once the best-fitting template was generated for a given patient, the visual scotoma could be projected onto the flattened cortex (Figure 4D). Further analysis of the BOLD signal was restricted to voxels within the projected ROI.

4.1.8. Comparing visual fields to fMRI data—The pattern standard deviation (PSD) scores on the SAP printout provides a global index that indicates a localized component in the deviation in decibels from the age-corrected normal values somewhere within the visual field. A comparison was made between the BOLD responses to the scotoma-mapping stimulus and the PSD from visual field testing for each patient. Increasingly positive PSD scores indicate a greater deviation from normal vision due to glaucoma. The PSD from both eyes of each patient was subtracted to yield a difference score (i.e., $PSD_{DIF} = PSD_{GLAUCOMATOUS} - PSD_{FELLOW\ EYE}$). The PSD_{DIF} scores were compared with the mean projected amplitudes from the scotoma-mapping experiments for all patients. Note that the amplitude of the BOLD response is a difference score itself, namely, the difference between viewing through the glaucomatous and fellow eyes. The BOLD response is not an absolute measure of neuronal activity for viewing through either eye, but rather a relative measure of the difference in neuronal activity associated with viewing through the glaucomatous vs. fellow eye.

4.1.9. Pointwise comparison of fMRI responses and visual fields—In addition to the analysis using global PSD_{DIF} scores, a “pointwise” comparison of thresholds throughout the visual field to fMRI responses in corresponding locations of V1 was also conducted. Apart from improving the statistical power by increasing the number of data points, this analysis also allows the relationship between visual function and brain responses to be assessed at retinotopically specific locations in the visual field rather than at the global level.

The pointwise analysis was restricted to the visual quadrant with the most damage as defined by the SAP visual field results. For each patient, twelve test locations from the quadrant of interest were projected onto the flattened representation of V1 via the best-fitting template (excluding the blindspot and the two most temporal test locations). The diameter of the projected test locations was 6°. The fMRI data was compared to visual function thresholds at each of the 12 test locations for all patients. The PD value at a given test location for the fellow eye was subtracted from that for the glaucomatous eye. The resulting PD_{DIF} score was then compared to the amplitude of the BOLD response for the voxels within the corresponding ROI. The total possible number of comparisons was 72 (6 patients × 12 test locations). However, five data points were omitted from the final analysis because reliable projected amplitudes from the fMRI data could not be obtained (an effect of having less than one voxel in a given ROI). Additionally, two outliers with low statistical leverage were identified and removed by plotting confidence intervals around the regression residuals (Osborne and Overbay, 2004).

4.1.10. Control experiments—Three control experiments were performed to determine whether any correlations could have occurred by chance. All three control experiments used data from the main experiments. However, the analysis for each control experiment was different.

In the first control experiment, the objective was to determine whether a correlation existed between the fMRI data and visual function data from the quadrant with the *least* amount of vision loss (as determined by the number of significant PD values). These quadrants are marked with asterisks in Figure 2. A correlation was not expected because the PD_{DIF} values for the relatively unaffected quadrant should not predict the observed BOLD responses. The analysis was conducted using the same BOLD data from the pointwise ROIs. However, for each patient, the BOLD data was randomly paired to the PD_{DIF} value from a random location in the less affected quadrant.

In the second control experiment, a statistical bootstrapping method was used to compute the probability of observing a correlation in the original pointwise comparison by chance (Henderson, 2005;Hesterberg et al., 2005). The population of PD_{DIF} values was randomly paired with the BOLD data from the pointwise ROIs. The correlation for this random sample was computed, and the process was repeated 10,000 times. The odds of getting the observed correlation were computed as follows. First, the number of random correlations that exceeded the observed correlation was counted. The total number of sample correlations then divided that number. The resulting p-value indicates the odds of getting the correlation by chance given the sample population.

The third control experiment was conducted to determine whether between-patient variability or within-patient variability could account for any correlations observed in the original pointwise comparison. A statistical bootstrapping approach similar to that of the second control experiment was used. For each patient, the BOLD data from the pointwise ROIs was randomly paired with the PD_{DIF} values from the quadrant with the greatest visual loss. Unlike the second control experiment, random pairings between the visual function and fMRI data occurred *within* patients. Correlations were computed for 10,000 random pairings, and the probability of getting the observed correlations was computed. If the majority of the total variability in the observed correlations could be attributed to between-patient variability, then randomizing the data within patients should have no affect on the correlation values. By contrast, if within-subject variability accounts for a significant portion of the total variability in the observed correlations, then the correlation value, *r*, should be greatly affected by randomization. Within-patient variability was expected to account for a significant portion of the variability in the observed. Thus, compared to the random correlations generated by the bootstrapping process, it was predicted that getting the observed correlations by chance was unlikely.

4.2. Results

4.2.1.FMRI data from a single patient—The glaucoma patients in this study had varying degrees of asymmetry between the glaucomatous and fellow eyes. This variability allowed us to make comparisons between visual field defects and brain activity across patients. The visual fields for each eye of the glaucoma patients are presented in Figure 2. To better illustrate the methods and results, the data from the patient 6 in Figure 2 is used as an example. This patient had severe visual loss in the right eye, particularly in the superior-nasal visual field. The bold line superimposed upon the data for the right eye describes the scotoma selected by the experimenter, which includes PD points that were statistically different from normal (95% confidence level). The complementary visual quadrant for the left eye is relatively normal. The experimenter restricted visual scotomas to one visual quadrant because the field of view available during the MRI experiments was limited.

FMRI responses to retinotopic mapping stimuli for this patient appear in Figure 4. The grayscale images in each panel show BOLD activity maps (i.e., projected amplitudes) on the flattened representation of the right hemisphere. The flattening in each panel is identical, but the pattern of BOLD activity depends upon which visual stimulus was presented. Bright regions correspond to locations where changes in BOLD signal correlate positively in time with the

stimulus phase (e.g., “on” vs. “off”). The ring-shaped activity (Figure 4A) indicates the BOLD response to the 16° isopter stimuli presented in the left visual hemifield. Responses to the arc presented in the left-superior visual field were averaged with responses to the arc presented in the left-inferior visual field. This ring-shaped pattern of activity extends beyond V1 into dorsal and ventral extrastriate cortex (V2, V3, V4, and V3a). The red line represents the corresponding component of the best-fitting template for that hemisphere. Similarly, responses to the meridian-mapping stimuli are depicted in Figure 4B-D. The “bow tie” and “hour glass” checkerboard patterns that make up the meridian-mapping stimulus were presented in alternation every 20 s, resulting in one BOLD activity map. The superior (Figure 4B) and inferior (Figure 4C) vertical meridians were fit independently and the best-fitting components from the template are superimposed upon the data (light and dark green respectively). The sign of the BOLD responses were reversed to fit responses to stimulation of the horizontal meridian (Figure 4D). The final best-fitting template for this patient is superimposed upon the BOLD responses to the vertical meridian (Figure 4E).

Once the best-fitting template was computed, viewing through the glaucomatous and fellow eye could be compared for this patient (Figure 5, Patient 6). The average BOLD responses to the scotoma-mapping stimulus in the third session are projected onto the flattened representation. The patient alternately viewed the stimulus through the glaucomatous or fellow eye in 20 s intervals. The phase of the BOLD response in relation to the temporal phase of monocular viewing is indicated by the color of the pixels. In this example, yellowish pixels correspond to voxels where viewing through the glaucomatous eye resulted in a larger amplitude signal than viewing through the fellow eye. That is to say, fMRI responses were “in phase” with the glaucomatous eye. Bluish pixels correspond to voxels that were in phase with the fellow eye. The best-fitting template for this patient is superimposed upon the BOLD responses along with a projection of the visual scotoma (black line). Most of the voxels within this ROI are blue, which indicates that BOLD responses in the ROI were in phase with viewing through the fellow eye. The mean projected amplitude of these voxels indicates the strength of the response. Viewing through the fellow eye was predicted to generate larger responses than viewing through the glaucomatous eye. For this patient, the mean projected amplitude across eight scans was significantly different from zero in the direction predicted by the hypothesis (t-test, $p < 0.0001$). Hence, the pattern of visual field loss observed using SAP is reflected by the pattern of BOLD activity in V1.

4.2.2. FMRI responses correlate with visual function thresholds—FMRI responses to the scotoma-mapping stimulus are plotted as the percent change in BOLD amplitude for all six patients (Figure 6A). FMRI responses from Figure 5 appear here with the same patient numbering scheme. Visual scotomas for each patient were projected onto the flattened representations of their corresponding hemispheres, and the resulting projections were defined as ROIs. The mean phase and amplitude of the voxels within the ROIs were correlated with the stimulus time course to yield projected amplitudes. Mean amplitudes were obtained by averaging projected amplitudes across eight scans per patient. Because visual field loss occurs in different eyes for each patient, the sign of the BOLD response was normalized (multiplied by 1 or −1) across patients. In Figure 6A, positive numbers indicate that the BOLD signal was in the predicted direction and viewing through the fellow eye evoked a larger cortical response than viewing through the glaucomatous eye. Negative numbers indicate that viewing through the glaucomatous eye resulted in larger mean projected amplitudes. All six patients demonstrated a significantly positive change in the BOLD amplitude, which denotes that viewing through the fellow eye elicited a greater fMRI response in V1 (t-test, all $p < 0.05$). Thus, in addition to the agreement between the pattern of visual field loss and the pattern of BOLD activity in cortex, there is also a significantly greater response in the ROI for viewing through the fellow eye.

The BOLD responses to the scotoma-mapping stimulus and the PSD_{DIF} scores from visual field testing were compared for each patient (Figure 6B). There was a positive correlation between the magnitude of a patient's PSD_{DIF} score from SAP and the change in their BOLD response ($r = 0.91$; $p = 0.01$). Thus, patients with a large difference in visual sensitivity between the glaucomatous eye and the fellow eye also demonstrated a greater difference between BOLD responses for viewing the scotoma-mapping stimulus through glaucomatous and fellow eyes.

4.2.3. Pointwise comparison of FMRI responses and visual function thresholds

—The results of the pointwise analysis are presented in Figure 7. The fMRI data for patient 6 in Figure 5 is presented along with the best-fitting template for this patient (Figure 7A). The location of each projected ROI (black circles) corresponds to one of twelve test locations in SAP. Because cortical magnification decreases with increasing eccentricity from the fovea, ROIs corresponding to test locations in the periphery are smaller than foveal ROIs. However, this difference does not present a problem for the analysis because differences in cortical magnification between individuals are accounted for by each patient's template. PD_{DIF} scores from all 12 test locations in the visual field were each compared to the amplitude of the BOLD response for the voxels within the corresponding ROI (Figure 7B). The pointwise analysis revealed a correlation between the change in amplitude of the BOLD response and PD_{DIF} scores derived from SAP ($r = 0.53$, $p < 0.0001$). This result remained significant when the analysis was completed with the two outliers ($r = 0.34$, $p = 0.0043$).

4.2.4. Control experiments

1. When the BOLD responses from the pointwise ROIs were randomly paired with the PD_{DIF} scores from the quadrant with the *least* amount of vision loss in the glaucomatous eye, there was no evidence of a correlation between the BOLD responses and the PD_{DIF} scores for SAP ($r = 0.19$, $p = 0.13$).
2. Additionally, when the pairing between the BOLD responses and the PD_{DIF} scores from the quadrant with the *greatest* loss was randomized, the probability of getting the observed correlations by chance was extremely rare (all $p < 0.0001$).
3. BOLD responses and PD_{DIF} scores for the quadrant with the greatest visual loss were also randomly paired *within* each patient. Relative to the population of random correlations, the probability of getting the observed correlation for SAP ($p < 0.0001$) was rare. Hence, there is evidence to suggest a significant portion of the total variability in the observed pointwise correlations is due to the variability within-patients.

5. Sources of potential error

5.1 Sources of potential error in template fitting

There are potential sources of error in the template fitting approach that have been discussed in detail elsewhere (Duncan and Boynton, 2003). In brief, the template is a simplified summary of the fMRI data, which is necessarily imperfect. Templates describe the basic features of the retinotopic map by minimizing the many sources of noise in the signal. It has been previously shown that these sources of noise do not introduce systematic biases into the mapping procedure (Duncan and Boynton, 2003). Some of these issues are discussed below.

5.1.1. The visual stimulus and the reliability of the fitting procedure—In theory, cortical magnification may have affected estimates of the representation of the 16° isopter. Increasing the width of the 16° isopter stimulus expands the region of activation in V1. Due to the increased representation of the fovea in V1, this expansion of activity would be larger near the foveal representation, which could bias the estimates of the representation of the 16°

isopter toward the fovea. A previous study using healthy observers demonstrated that the width of such stimuli does not have a significant impact on the template fitting approach (Duncan and Boynton, 2003). In that study, fits to the activity patterns elicited by rings with very different widths were nearly identical, indicating that estimates of peak activity correspond to the actual stimulus representation on the cortex.

In general, the fMRI response is reliable and repeatable within a 3×3×3 mm voxel (Garcia-Alvarez et al., 2006). Unfortunately, there were not enough subjects or repeats in the current study to do a split-half reliability test. Nevertheless, a previous study comparing cortical magnification in V1 to visual acuity determined that the template fitting method was reliable and repeatable using nearly identical stimuli (Duncan and Boynton, 2003). In that study, the correlation between acuity and cortical magnification was significant for both hemispheres/hemifields when analyzed independently. The correlation was also significant using both the first and last half of the fMRI sessions. These two split-half reliability tests indicate that the location of the fMRI response to the visual stimuli and the template fitting method are repeatable and reliable.

A majority of the activity visible in the flattened representation could be attributed to hemodynamic blurring, a spatially diffuse response that is roughly Gaussian and is not spatially biased in a manner that could affect the fits. Hemodynamic blurring originates from multiple sources. First, the BOLD signal is known to extend beyond the focus of neuronal activation (Grinvald et al., 1994). Second, the spatial sampling of the fMR images (3×3×3 mm resolution) exaggerates the extent of the signal via partial volume effects. Finally, to smooth the response on the flattened cortex, parameter maps on the flattened representation of the cortex were blurred with a Gaussian filter (width at half-height = 1/e). These sources of spatial blurring only affect the extent of measured activity, but not the location of the peak. Accordingly, the error associated with estimating a point in visual space from a point on the flattened representation has been shown to be less than +/− 4.6 minutes of visual angle at 1.5° eccentricity and +/− 27 min at 12° (Duncan and Boynton, 2003).

5.1.2. Distortions in the cortical flattening technique—An iterative method was used to project locations from the 3D anatomical reference volume of each patient's brain onto a 2D surface (Wandell et al., 2000). Minor distortions are inherent in this process because the surface of the brain is not topologically equivalent to a plane. A plane better approximates smaller areas of a smooth curved surface than it does larger areas. Therefore, flattening the smallest region possible minimized distortions. The flattening technique results in approximately +/− 10% distortion with a roughly equal amount of compression and expansion (Duncan and Boynton, 2003). Hence, it is unlikely that this method of cortical flattening would introduce a systematic bias in the estimates of V1 topography in glaucoma patients.

5.1.3. Fixation losses—Several steps were taken to ensure that patients were fixating appropriately. Although patients did not report any difficulty with fixation using either eye, the fixation target in the fMRI experiments was larger than used typically with standard diagnostic tests. Moreover, there was no indication with eye tracking that the subjects had any difficulty performing the fixation task as instructed. Finally, acuity in all six glaucoma subjects was 20/40 or better in both eyes.

It is highly unlikely that fixation losses had a negative impact on the results. Failure to fixate properly during the fMRI portion of the experiment theoretically could result in a lack of clear retinotopy and a weaker correlation between fMRI and structure/function. Moreover, fixation losses add noise to the fMRI responses, reducing the strength of the correlation. Hence, it is highly likely that the correlation between fMRI response and structure/function is greater than observed.

5.2. Sources of error in perimetric testing

The scotomas in all of the patients were repeatable across multiple visits. However, the first patient recruited (Patient 1, Figure 2) was originally tested using kinetic perimetry with the Octopus 101 (Haag Streit International, Koeniz-Berne, Switzerland). Kinetic perimetry indicated a scotoma in the inferior-nasal quadrant of the right eye. After kinetic perimetry, the patient participated in fMRI scanning, but further testing with SAP revealed a more prominent scotoma in the inferior-temporal field of the same eye (no visual field defect was detected at this location using kinetic perimetry). Because the patient was unavailable for further fMRI scanning, the original scotoma was used in the analysis. The visual field results showing inferior temporal and inferior nasal damage for this patient were also repeatable in subsequent visits with SAP. Due to the potential discrepancy between kinetic perimetry and SAP visual fields were evaluated with SAP.

To avoid confusion with the blindspot, visual scotomas were either located in the hemifield opposite the blindspot, or at least 6 degrees away from the horizontal meridian. The blindspot in normal observers is located about 15 degrees medial to the fovea and roughly 5 degrees in diameter. When measured using fMRI, the size of the blindspot on the flattened representation of visual cortex depends on the correlation threshold (Tootell et al., 1998). The template mapping techniques were used to determine the area of the region of cortex dedicated to the blindspot. The area of cortex dedicated to the blindspot for the patients in this study was 3.2 +/− 1.2 mm^2. For the patient with the smallest scotoma, the area of the representation of the blindspot was only 6% of that for the scotoma. For the patient with the largest scotoma, the area of the representation of the blindspot was only 1% of that for the scotoma. Note that the representation of the blindspot did not intersect the representation of the scotoma, and therefore voxels within the blindspot representation were not included in the analysis. Therefore, the cortical representation of the blindspot contributes little to the fMRI response compared to the representation of the visual scotomas.

5.3. Variability related to small sample sizes

The population of patients in this study had varying degrees of visual field loss. Originally, patients with extreme asymmetries were to be recruited (i.e., completely blind in one eye and no visual loss in the fellow eye), but such patients proved to be less common than anticipated. Nevertheless, the gradual continuum of asymmetries across patients proved to be an advantage. A lack of variability in the sample population would have prohibited us from detecting evidence of a correlation between visual fields and cortical responses in the between-subjects analysis. Still, the small number of strongly asymmetric patients encountered ultimately limited the sample size.

The increased sample size of the pointwise analysis resulted in significant correlations between cortical responses and results from visual function testing. However, the Pearson's correlation statistic appeared to be diminished relative to the between-subjects test, even though this difference was not statistically significant ($p = 0.113$). The apparent difference may have occurred because the two analyses used (1) a different number of ROIs and (2) a different number of test locations in the visual function tests. The between-subjects analysis used one large ROI whereas the pointwise analysis used 12 ROIs. Additionally, the between-subjects analysis compared the difference between global PSD scores for the whole visual field, whereas the pointwise analysis compared the difference between multiple PD scores within one quadrant. The global PSD score is not as spatially precise as the individual PD values. However, the lack of spatial resolution of the global PSD may be countermanded by the greater visual area contributing to the score.

While a larger number of subjects would improve quantitative estimates of the correlation between glaucomatous optic neuropathy and cortical damage in the current study, it is unlikely that an increase in subjects would change the results or the means by which the scotoma-mapping technique will be applied in future studies. The objective of this study was to demonstrate that the scotoma-mapping technique can be used to evaluate the extent of cortical damage in human glaucoma. More subjects are needed to provide better estimates of the extent of the damage at various stages of glaucoma.

6. Visual sensitivity predicts cortical responses in a retinotopic fashion

A ROI-based approach was used to compare fMRI responses and visual sensitivity thresholds at different locations in visual space. The difference in visual sensitivity between eyes was correlated with the difference in fMRI responses to visual stimulation of each eye. This study is the first to compare visual function to cortical function at specific and multiple locations throughout the visual field. The results from this study suggest that the ROI template-fitting technique can be used to quantify the effects of POAG on post-retinal mechanisms.

The correlation in the pointwise analysis supports the prediction that visual field thresholds in POAG are related to cortical responses in a retinotopic fashion. Three control experiments were conducted to test whether the correlations in the pointwise analysis could have arisen by chance. In one control experiment, the BOLD responses for all of the patients were randomly paired with the PD_{DIF} scores from a different patient. A statistical bootstrapping procedure indicated that the probability of getting the observed correlations by chance was unlikely. While this result assured us that the observed correlations were not spurious, the experiment has little to say about the retinotopic organization of the cortical responses. The results of the remaining control experiments bear directly on this hypothesis.

A second control experiment randomly paired BOLD responses from the pointwise ROIs to PD_{DIF} scores from the quadrant with the least amount of visual loss. There was no correlation between the BOLD responses and PD_{DIF} scores for SAP. These results support the notion that the relationship between cortical responses and visual function is retinotopic, and not merely a function of the overall visual ability of the patient.

In the third control experiment, the pairing between the PD_{DIF} scores and the BOLD responses from the pointwise ROIs was randomized *within* patients. Statistical bootstrapping revealed that within-subjects randomization had a significant effect on the correlation value. Hence, a significant proportion of the variability for this correlation can be attributed to within-patient variability. Together with the results of the main pointwise analysis and the first control experiment, these results support the notion that visual sensitivity in POAG is precisely correlated with cortical responses in a retinotopic fashion.

The third control experiment also provides information about the independence of the samples in the pointwise analysis. Two measures are generally considered independent if the probability of observing one does not depend on the presence of the other (Zar, 1999). The data points in the pointwise correlations (Figure 7B) might be considered independent observations because the ROI (specifically, the BOLD response from the voxels therein) is the unit being correlated with the PD_{DIF} values. On the other hand, several ROIs are correlated for each observer, which might be considered a violation of statistical independence. The third control experiment was designed to determine whether between-patient variability or within-patient variability could account for any correlations observed in the original pointwise comparison, which also addresses whether the data points in Figure 7 are independent. If randomizing the data within-subjects does not affect the probability of observing a significant correlation, then there is evidence to suggest that inter-observer variability accounts for most of the variability in the observed correlations and the data points should not be considered independent. However,

within-subject variability was determined to account for the variability in the observed correlations, and thus there is evidence to suggest that the data points in Figure 7B should be regarded as independent observations.

7. The role of fMRI in glaucoma research

FMRI may be a useful tool for glaucoma research as glaucoma is an optic neuropathy that affects the central nervous system as well as the eye. Understanding changes in human glaucoma may provide insights into the pathobiology of the disease. Specifically, fMRI may enhance our understanding of the process of transsynaptic degeneration, which occurs when injured neurons have unfavorable effects on pre- or post-synaptic neurons. Recently, transsynaptic degeneration has been implicated in animal models of glaucoma (Gupta and Yucel, 2001,2003). The death of retinal ganglion cells may prompt a cascade of events along the retino-cortical pathway that has neurochemical (Vickers et al., 1997), metabolic (Crawford et al., 2000;Crawford et al., 2001), functional (Smith et al., 1993), and neuropathological consequences for LGN and V1 such as neuron loss and shrinkage (Weber et al., 2000;Yucel et al., 2000;Yucel et al., 2001,2003).

It should be noted that fMRI measurements of changes in neuronal activity are not direct evidence for glaucomatous neurodegeneration in LGN or V1. It is possible to have functional changes in neuronal activity that are independent of structural changes to neurons/axons in the central nervous system and *vice versa*. For example, recent fMRI studies have found neuronal activity in the cortical representation of the fovea persists despite obvious macular pathology resulting in extensive losses to foveal vision (Nguyen et al., 2004a,b;Baker et al., 2005). Nevertheless, fMRI offers a great advantage over anatomical and electrophysiological methods that can directly measure neurodegeneration. Specifically, fMRI can measure glaucomatous changes to function-specific neuronal activity at several stages along the visual pathway *in vivo*. Such fMRI measurements may constrain future anatomical or electrophysiological studies.

Cell death in glaucoma is not necessarily limited to transsynaptic degeneration associated with the glaucomatous eye. There is also a decrease in the number and size of M and P cells receiving input from the non-glaucomatous eye in primate models (Yucel et al., 2003). “Sympathetic cell death” may occur at locations where neurons receiving inputs from both eyes lie adjacent to each other. The current study paves the way for a ROI-based approach to investigating sympathetic activity decreases in human glaucoma.

8. Future directions

Animal models of glaucoma suggest that retinal ganglion cell death adversely affects cells in V1 via transsynaptic degeneration. Yet, there is a paucity of evidence regarding the existence of such mechanisms in humans. To explore this possibility, fMRI can be used measure the influence of the glaucomatous eye on the processing of visual input from the relatively unaffected fellow eye. Cortical responses to visual stimulation in control subjects can be compared to responses driven by the fellow eye of asymmetric glaucoma subjects. Visual fields and structural measurements can be conducted to confirm that there is no detectible difference between normal eyes and the fellow eye of glaucoma subjects. According to predictions from animal models of glaucoma, visual stimulation of the unaffected fellow eye of glaucoma subjects should elicit V1 responses that are reduced relative to those of control subjects. Furthermore, fMRI measurements of neuronal activity in V1 will depend upon the severity of vision loss, changes to optic disk topography, and thinning of the retinal nerve fiber layer in glaucoma subjects. FMRI measurements of neuronal activity in V1 should also correlate with the loss of visual function at multiple locations in visual space.

Neurons within the layers of LGN receiving input from the unaffected fellow eye also show signs of degeneration, which implies that the death of LGN neurons connected to the glaucomatous eye creates a toxic environment affecting all LGN cells (Luthra et al., 2005). Detailed FMR imaging in the LGN has been achieved recently at 3.0 T (O'Connor et al., 2002;Kastner et al., 2004;Schneider et al., 2004). By measuring fMRI activity in the LGN, the presence of "sympathetic" cell death in human glaucoma may be verified. Such experiments may determine whether transsynaptic and sympathetic degeneration occur in LGN, V1, or both areas in human glaucoma. As such, visual stimulation of the unaffected fellow eye of glaucoma subjects should elicit LGN responses that are reduced relative to those of control subjects. Furthermore, FMRI measurements of neuronal activity in LGN should depend upon the severity of vision loss, changes to optic disk topography, and thinning of the retinal nerve fiber layer in glaucoma.

The combined outcome of experiments in LGN and V1 may enhance our understanding of the nature of neuronal activity in glaucoma. Given evidence of transsynaptic degeneration in V1, a lack of degeneration in LGN would imply that transsynaptic degeneration occurs in V1 in the absence of sympathetic cell death in LGN. Because the optic nerve fibers from each eye are functionally and anatomically segregated in LGN (Wiesel and Hubel, 1966;Dreher et al., 1976;Creutzfeldt et al., 1979;Shapley et al., 1981;Merigan and Maunsell, 1993), it is possible that selective cell death could occur in one layer of LGN without affecting the others. This pattern of results would also rule out the possibility that retinal ganglion cell loss in the fellow eye could account for transsynaptic degeneration in V1. By contrast, evidence of degeneration in LGN and V1 suggests that each mechanism occurs at both stages of visual processing. However, it would not be possible to determine which mechanism was responsible for cell death in LGN. Finally, evidence of degeneration in LGN alone would indicate that both mechanisms may be present but the effects of transsynaptic degeneration are undetectable in V1.

Using the template-fitting approach, the current experiment establishes a strong correlation between the size and severity of a given scotoma and the pattern and amplitude of the BOLD response within its corresponding ROI. Despite these encouraging results, template-fitting techniques can be improved upon. First, cortical flattening introduces small, unbiased errors that add noise to the correlation. To overcome this problem, a recently developed template-fitting method measures cortical distance along the 3-D cortical manifold (Dougherty et al., 2003). Second, the series of static stimuli used in the current study require nearly one hour to define the landmarks in V1 necessary for template-fitting. Advances in multifocal fMRI (Vanni et al., 2005) utilize multiple static stimuli and m-sequences (pseudorandom sequences designed to maximize stimulus presentation efficiency) to create a 60-piece grid in V1. While current multifocal fMRI methods have a relatively poor signal-to-noise ratio, the time saved using these techniques may prove beneficial for scanning elderly glaucoma patients.

Similar to recent reports of functional reorganization in patients with macular degeneration (Nguyen et al., 2004a,b;Baker et al., 2005), functional reorganization may occur within V1 in response to glaucoma, and the cortical representation of the fellow eye could theoretically grow to include the cortical representation of the glaucomatous eye. As a result, neuronal activity in V1 might be increased for viewing through the fellow eye relative to normal control subjects. This report has assumed that cortical responses to viewing through the fellow eye are relatively unchanged compared to healthy control subjects. Because the BOLD response is a relative measure of viewing through the glaucomatous vs. the fellow eye, it is not possible to determine how much of the BOLD response can be attributed to changes in neuronal activity associated with viewing through the fellow eye. Future studies are planned to compare the BOLD response to normal controls, which will directly address the issue of cortical plasticity.

9. Conclusion

As experimental models of glaucoma do not fully mimic human POAG, careful study of human patients is needed. The fMRI techniques developed in this report can be used to study human glaucoma *in vivo*. Such endeavors may lead to new approaches for diagnosing and treating this neurodegenerative disease.

Acknowledgements

The authors would like to thank Neeru Gupta, M.D., PhD, FRCSC, DABO, and Thomas T. Liu, Ph.D., for their insightful comments on this manuscript.

References

Baker CI, Peli E, Knouf N, Kanwisher NG. Reorganization of visual processing in macular degeneration. J Neurosci 2005;25:614–618. [PubMed: 15659597]

Bandettini PA, Wong EC, Hinks RS, Tikofsky RS, Hyde JS. Time course EPI of human brain function during task activation. Magn Reson Med 1992;25:390–397. [PubMed: 1614324]

Bedwell JS, Miller LS, Brown JM, McDowell JE, Yanasak NE. Functional magnetic resonance imaging examination of the magnocellular visual pathway in nonpsychotic relatives of persons with schizophrenia. Schizophr Res 2004;71:509–510. [PubMed: 15474923]

Brainard DH. The Psychophysics Toolbox. Spat Vis 1997;10:433–436. [PubMed: 9176952]

Brodsky MC, Glasier CM, Creel DJ. Magnetic resonance imaging of the visual pathways in human albinos. J Pediatr Ophthalmol Strabismus 1993;30:382–385. [PubMed: 8120744]

Buxton, RB. Introduction to functinal magnetic resonance imaging: Principles and techniques. New York: Cambridge University Press; 2002.

Chaturvedi N, Hedley-Whyte ET, Dreyer EB. Lateral geniculate nucleus in glaucoma. Am J Ophthalmol 1993;116:182–188. [PubMed: 8352303]

Crawford ML, Harwerth RS, Smith EL 3rd, Shen F, Carter-Dawson L. Glaucoma in primates: cytochrome oxidase reactivity in parvo- and magnocellular pathways. Invest Ophthalmol Vis Sci 2000;41:1791–1802. [PubMed: 10845600]

Crawford ML, Harwerth RS, Smith EL 3rd, Mills S, Ewing B. Experimental glaucoma in primates: changes in cytochrome oxidase blobs in V1 cortex. Invest Ophthalmol Vis Sci 2001;42:358–364. [PubMed: 11157867]

Creutzfeldt OD, Lee BB, Elepfandt A. A quantitative study of chromatic organisation and receptive fields of cells in the lateral geniculate body of the rhesus monkey. Exp Brain Res 1979;35:527–545. [PubMed: 110613]

Dale AM, Sereno MI. Combining EEG and MEG with MRI cortical surface reconstruction: a linear approach. J Cogn Neurosci 1993;5:162–176.

Demb JB, Boynton GM, Best M, Heeger DJ. Psychophysical evidence for a magnocellular pathway deficit in dyslexia. Vision Res 1998;38:1555–1559. [PubMed: 9747491]

DeYoe EA, Bandettini P, Neitz J, Miller D, Winans P. Functional magnetic resonance imaging (FMRI) of the human brain. J Neurosci Methods 1994;54:171–187. [PubMed: 7869750]

DeYoe EA, Carman GJ, Bandettini P, Glickman S, Wieser J, Cox R, Miller D, Neitz J. Mapping striate and extrastriate visual areas in human cerebral cortex. Proc Natl Acad Sci U S A 1996;93:2382–2386. [PubMed: 8637882]

Dougherty RF, Koch VM, Brewer AA, Fischer B, Modersitzki J, Wandell BA. Visual field representations and locations of visual areas V1/2/3 in human visual cortex. J Vis 2003;3:586–598. [PubMed: 14640882]

Dreher B, Fukada Y, Rodieck RW. Identification, classification and anatomical segregation of cells with X-like and Y-like properties in the lateral geniculate nucleus of old-world primates. J Physiol 1976;258:433–452. [PubMed: 822151]

Duncan RO, Boynton GM. Cortical magnification within human primary visual cortex correlates with acuity thresholds. Neuron 2003;38:659–671. [PubMed: 12765616]

Engel SA, Glover GH, Wandell BA. Retinotopic organization in human visual cortex and the spatial precision of functional MRI. Cereb Cortex 1997;7:181–192. [PubMed: 9087826]

Engel SA, Rumelhart DE, Wandell BA, Lee AT, Glover GH, Chichilnisky EJ, Shadlen MN. fMRI of human visual cortex. Nature 1994;369:525. [PubMed: 8031403]

Fortune B, Hood DC. Conventional pattern-reversal VEPs are not equivalent to summed multifocal VEPs. Invest Ophthalmol Vis Sci 2003;44:1364–1375. [PubMed: 12601070]

Frahm J, Bruhn H, Merboldt KD, Hanicke W. Dynamic MR imaging of human brain oxygenation during rest and photic stimulation. J Magn Reson Imaging 1992;2:501–505. [PubMed: 1392241]

Fujita N, Tanaka H, Takanashi M, Hirabuki N, Abe K, Yoshimura H, Nakamura H. Lateral geniculate nucleus: anatomic and functional identification by use of MR imaging. AJNR Am J Neuroradiol 2001;22:1719–1726. [PubMed: 11673167]

Garcia-Alvarez R, Liney GP, Beavis AW. Repeatability of functional MRI for conformal avoidance radiotherapy planning. J Magn Reson Imaging 2006;23:108–114. [PubMed: 16416436]

Goldberg I, Graham SL, Klistorner AI. Multifocal objective perimetry in the detection of glaucomatous field loss. Am J Ophthalmol 2002;133:29–39. [PubMed: 11755837]

Graham SL, Klistorner AI, Goldberg I. Clinical application of objective perimetry using multifocal visual evoked potentials in glaucoma practice. Arch Ophthalmol 2005;123:729–739. [PubMed: 15955974]

Graham SL, Klistorner AI, Grigg JR, Billson FA. Objective VEP perimetry in glaucoma: asymmetry analysis to identify early deficits. J Glaucoma 2000;9:10–19. [PubMed: 10708226]

Grinvald A, Lieke EE, Frostig RD, Hildesheim R. Cortical point-spread function and long-range lateral interactions revealed by real-time optical imaging of macaque monkey primary visual cortex. J Neurosci 1994;14:2545–2568. [PubMed: 8182427]

Gupta N, Yucel YH. Glaucoma and the brain. J Glaucoma 2001;10:S28–29. [PubMed: 11890268]

Gupta N, Yucel YH. Brain changes in glaucoma. Eur J Ophthalmol 2003;13(Suppl 3):S32–35. [PubMed: 12749675]

Gupta N, Ang LC, Noel de Tilly L, Bidaisee L, Yucel YH. Human glaucoma and neural degeneration in intracranial optic nerve, lateral geniculate nucleus, and visual cortex. Br J Ophthalmol 2006;90:674–678. [PubMed: 16464969]

Harwerth RS, Quigley HA. Visual field defects and retinal ganglion cell losses in patients with glaucoma. Arch Ophthalmol 2006;124:853–859. [PubMed: 16769839]

Harwerth RS, Carter-Dawson L, Shen F, Smith EL 3rd, Crawford ML. Ganglion cell losses underlying visual field defects from experimental glaucoma. Invest Ophthalmol Vis Sci 1999;40:2242–2250. [PubMed: 10476789]

Hasegawa S, Ohshima A, Hayakawa Y, Takagi M, Abe H. Multifocal electroretinograms in patients with branch retinal artery occlusion. Invest Ophthalmol Vis Sci 2001;42:298–304. [PubMed: 11133882]

Henderson AR. The bootstrap: a technique for data-driven statistics. Using computer-intensive analyses to explore experimental data. Clin Chim Acta 2005;359:1–26. [PubMed: 15936746]

Hesterberg, T.; Moore, DS.; Monaghan, S.; Clipson, A.; Epstein, R. Bootstrap methods and permutation tests. 2. New York: W. H. Freeman; 2005.

Hood DC, Greenstein VC. Multifocal VEP and ganglion cell damage: applications and limitations for the study of glaucoma. Prog Retin Eye Res 2003;22:201–251. [PubMed: 12604058]

Hood DC, Zhang X, Greenstein VC, Kangovi S, Odel JG, Liebmann JM, Ritch R. An interocular comparison of the multifocal VEP: a possible technique for detecting local damage to the optic nerve. Invest Ophthalmol Vis Sci 2000;41:1580–1587. [PubMed: 10798679]

Hood DC, Thienprasiddhi P, Greenstein VC, Winn BJ, Ohri N, Liebmann JM, Ritch R. Detecting early to mild glaucomatous damage: a comparison of the multifocal VEP and automated perimetry. Invest Ophthalmol Vis Sci 2004;45:492–498. [PubMed: 14744890]

Johnson CA, Sample PA, Zangwill LM, Vasile CG, Cioffi GA, Liebmann JR, Weinreb RN. Structure and function evaluation (SAFE): II. Comparison of optic disk and visual field characteristics. Am J Ophthalmol 2003;135:148–154. [PubMed: 12566017]

Kastner S, O'Connor DH, Fukui MM, Fehd HM, Herwig U, Pinsk MA. Functional imaging of the human lateral geniculate nucleus and pulvinar. J Neurophysiol 2004;91:438–448. [PubMed: 13679404]

Kiyosawa M, Bosley TM, Kushner M, Jamieson D, Alavi A, Savino PJ, Sergott RC, Reivich M. Positron emission tomography to study the effect of eye closure and optic nerve damage on human cerebral glucose metabolism. Am J Ophthalmol 1989;108:147–152. [PubMed: 2787961]

Kleinschmidt A, Lee BB, Requardt M, Frahm J. Functional mapping of color processing by magnetic resonance imaging of responses to selective P- and M-pathway stimulation. Exp Brain Res 1996;110:279–288. [PubMed: 8836691]

Klistorner AI, Graham SL, Grigg JR, Billson FA. Multifocal topographic visual evoked potential: improving objective detection of local visual field defects. Invest Ophthalmol Vis Sci 1998;39:937–950. [PubMed: 9579473]

Krauzlis RJ, Miles FA. Initiation of saccades during fixation or pursuit: evidence in humans for a single mechanism. J Neurophysiol 1996;76:4175–4179. [PubMed: 8985910]

Kwong KK, Belliveau JW, Chesler DA, Goldberg IE, Weisskoff RM, Poncelet BP, Kennedy DN, Hoppel BE, Cohen MS, Turner R, et al. Dynamic magnetic resonance imaging of human brain activity during primary sensory stimulation. Proc Natl Acad Sci U S A 1992;89:5675–5679. [PubMed: 1608978]

Liu J, Wandell BA. Specializations for chromatic and temporal signals in human visual cortex. J Neurosci 2005;25:3459–3468. [PubMed: 15800201]

Luthra A, Gupta N, Kaufman PL, Weinreb RN, Yucel YH. Oxidative injury by peroxynitrite in neural and vascular tissue of the lateral geniculate nucleus in experimental glaucoma. Exp Eye Res 2005;80:43–49. [PubMed: 15652525]

Merigan WH, Maunsell JH. How parallel are the primate visual pathways? Annu Rev Neurosci 1993;16:369–402. [PubMed: 8460898]

Miki A, Nakajima T, Takagi M, Shirakashi M, Abe H. Detection of visual dysfunction in optic atrophy by functional magnetic resonance imaging during monocular visual stimulation. Am J Ophthalmol 1996;122:404–415. [PubMed: 8794713]

Nguyen TH, Stievenart JL, Saucet JC, Le Gargasson JF, Cohen YS, Pelegrini-Issac M, Burnod Y, Iba-Zizen MT, Cabanis EA. Cortical response to age-related macular degeneration (Part II). Functional MRI study. J Fr Ophtalmol 2004a;27:3S72–86. [PubMed: 15602409]

Nguyen TH, Stievenart JL, Saucet JC, Le Gargasson JF, Cohen YS, Pelegrini-Issac M, Burnod Y, Iba-Zizen MT, Cabanis EA. Cortical response in age-related macular degeneration (part I). Methodology and subject specificities. J Fr Ophtalmol 2004b;27:3S65–71. [PubMed: 15602408]

O'Connor DH, Fukui MM, Pinsk MA, Kastner S. Attention modulates responses in the human lateral geniculate nucleus. Nat Neurosci 2002;5:1203–1209. [PubMed: 12379861]

Ogawa S, Lee TM, Nayak AS, Glynn P. Oxygenation-sensitive contrast in magnetic resonance image of rodent brain at high magnetic fields. Magn Reson Med 1990;14:68–78. [PubMed: 2161986]

Ogawa S, Tank DW, Menon R, Ellermann JM, Kim SG, Merkle H, Ugurbil K. Intrinsic signal changes accompanying sensory stimulation: functional brain mapping with magnetic resonance imaging. Proc Natl Acad Sci U S A 1992;89:5951–5955. [PubMed: 1631079]

Osborne JW, Overbay A. The power of outliers (and why researchers should always check for them). Practical Assessment, Research & Evaluation 2004;9

Pelli DG. The VideoToolbox software for visual psychophysics: transforming numbers into movies. Spat Vis 1997;10:437–442. [PubMed: 9176953]

Quigley HA, Broman AT. The number of people with glaucoma worldwide in 2010 and 2020. Br J Ophthalmol 2006;90:262–267. [PubMed: 16488940]

Schneider KA, Richter MC, Kastner S. Retinotopic organization and functional subdivisions of the human lateral geniculate nucleus: a high-resolution functional magnetic resonance imaging study. J Neurosci 2004;24:8975–8985. [PubMed: 15483116]

Schneider W, Noll DC, Cohen JD. Functional topographic mapping of the cortical ribbon in human vision with conventional MRI scanners. Nature 1993;365:150–153. [PubMed: 8371756]

Schwartz EL. A quantitative model of the functional architecture of human striate cortex with application to visual illusion and cortical texture analysis. Biol Cybern 1980;37:63–76. [PubMed: 6772241]

Sereno MI, Dale AM, Reppas JB, Kwong KK, Belliveau JW, Brady TJ, Rosen BR, Tootell RB. Borders of multiple visual areas in humans revealed by functional magnetic resonance imaging. Science 1995;268:889–893. [PubMed: 7754376]

Shapley R, Kaplan E, Soodak R. Spatial summation and contrast sensitivity of X and Y cells in the lateral geniculate nucleus of the macaque. Nature 1981;292:543–545. [PubMed: 7254350]

Smith IELI, Chino YM, Harwerth RS, Rider WHI, Crawford ML. Retinal inputs to the monkey's lateral geniculate nucleus in experimental glaucoma. Clin Vis Sci 1993;8:113–139.

Sommer A, Katz J, Quigley HA, Miller NR, Robin AL, Richter RC, Witt KA. Clinically detectable nerve fiber atrophy precedes the onset of glaucomatous field loss. Arch Ophthalmol 1991;109:77–83. [PubMed: 1987954]

Sugiyama T, Utsunomiya K, Ota H, Ogura Y, Narabayashi I, Ikeda T. Comparative study of cerebral blood flow in patients with normal-tension glaucoma and control subjects. Am J Ophthalmol 2006;141:394–396. [PubMed: 16458708]

Thienprasiddhi P, Greenstein VC, Chen CS, Liebmann JM, Ritch R, Hood DC. Multifocal visual evoked potential responses in glaucoma patients with unilateral hemifield defects. Am J Ophthalmol 2003;136:34–40. [PubMed: 12834667]

Tootell RB, Hadjikhani NK, Vanduffel W, Liu AK, Mendola JD, Sereno MI, Dale AM. Functional analysis of primary visual cortex (V1) in humans. Proc Natl Acad Sci U S A 1998;95:811–817. [PubMed: 9448245]

Vanni S, Henriksson L, James AC. Multifocal fMRI mapping of visual cortical areas. Neuroimage 2005;27:95–105. [PubMed: 15936956]

Vickers JC, Hof PR, Schumer RA, Wang RF, Podos SM, Morrison JH. Magnocellular and parvocellular visual pathways are both affected in a macaque monkey model of glaucoma. Aust N Z J Ophthalmol 1997;25:239–243. [PubMed: 9296301]

Wandell BA, Chial S, Backus BT. Visualization and measurement of the cortical surface. J Cogn Neurosci 2000;12:739–752. [PubMed: 11054917]

Wandell BA, Poirson AB, Newsome WT, Baseler HA, Boynton GM, Huk A, Gandhi S, Sharpe LT. Color signals in human motion-selective cortex. Neuron 1999;24:901–909. [PubMed: 10624953]

Weber AJ, Chen H, Hubbard WC, Kaufman PL. Experimental glaucoma and cell size, density, and number in the primate lateral geniculate nucleus. Invest Ophthalmol Vis Sci 2000;41:1370–1379. [PubMed: 10798652]

Weinreb RN, Khaw PT. Primary open-angle glaucoma. Lancet 2004;363:1711–1720. [PubMed: 15158634]

Weinreb RN, Lindsey JD, Sample P. Lateral geniculate nucleus in glaucoma. Am J Ophthalmol 1994;118:126–129. [PubMed: 8023870]

Wiesel TN, Hubel DH. Spatial and chromatic interactions in the lateral geniculate body of the rhesus monkey. J Neurophysiol 1966;29:1115–1156. [PubMed: 4961644]

Yoshida Y, Sugiyama T, Sugasawa J, Nakajima M, Ikeda T, Utsunomiya K. A case of normal-tension glaucoma with impaired eye movements in a young patient. Nippon Ganka Gakkai Zasshi 2006;110:477–483. [PubMed: 16808164]

Yucel YH, Zhang Q, Gupta N, Kaufman PL, Weinreb RN. Loss of neurons in magnocellular and parvocellular layers of the lateral geniculate nucleus in glaucoma. Arch Ophthalmol 2000;118:378–384. [PubMed: 10721961]

Yucel YH, Zhang Q, Weinreb RN, Kaufman PL, Gupta N. Atrophy of relay neurons in magno- and parvocellular layers in the lateral geniculate nucleus in experimental glaucoma. Invest Ophthalmol Vis Sci 2001;42:3216–3222. [PubMed: 11726625]

Yucel YH, Zhang Q, Weinreb RN, Kaufman PL, Gupta N. Effects of retinal ganglion cell loss on magno-, parvo-, koniocellular pathways in the lateral geniculate nucleus and visual cortex in glaucoma. Prog Retin Eye Res 2003;22:465–481. [PubMed: 12742392]

Zar, JH. Biostatistical analysis. 4. New Jersey: Prentice Hall; 1999.

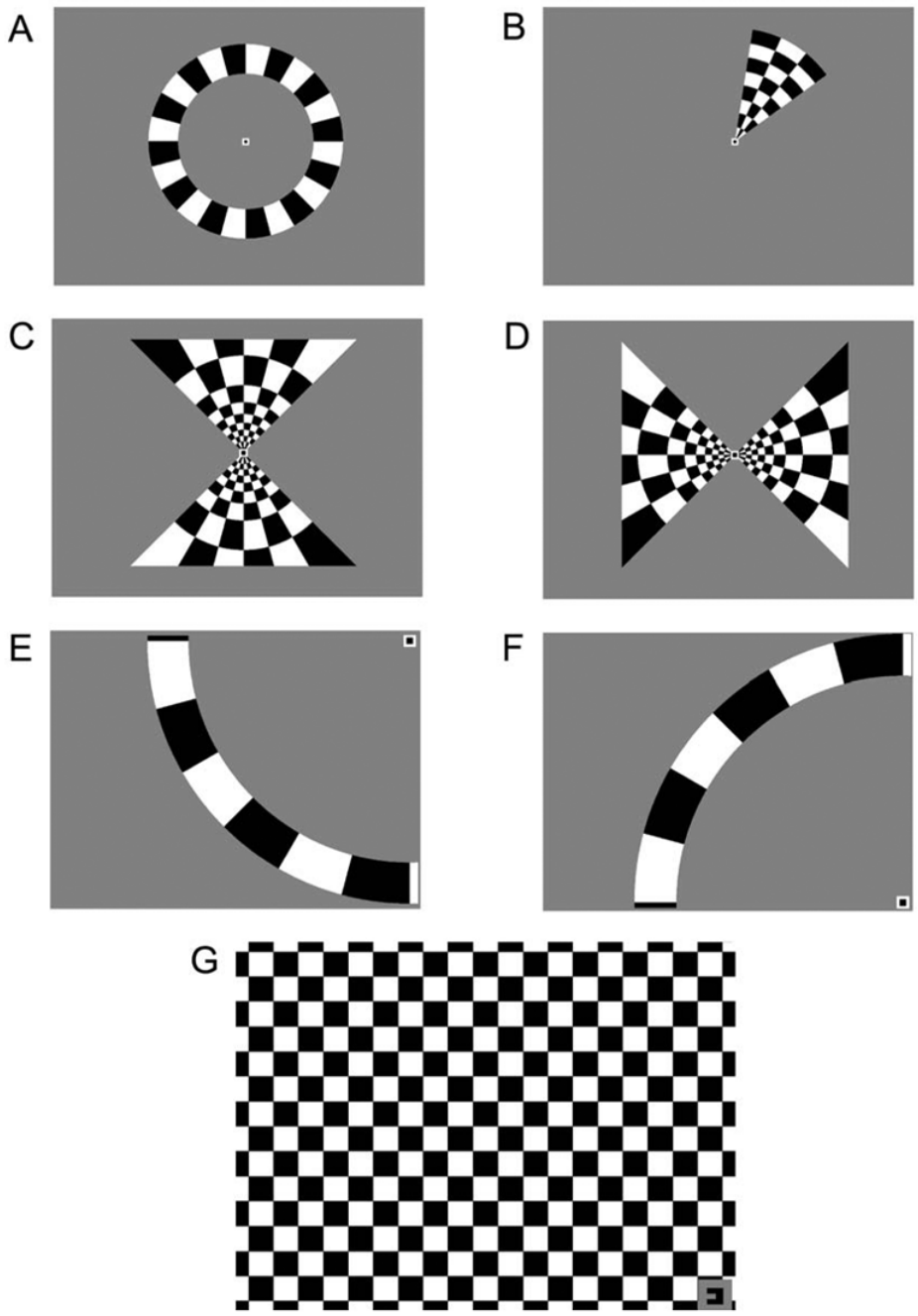

Figure 1. Visual Stimuli for FMRI Experiments

Several stimuli (***A***–***F***) were used to obtain retinotopic maps of the visual world on the flattened cortex of the patients. Patients fixated on a stationary target while contrast-reversing checkerboard patterns (100% contrast; 8 Hz flicker) were presented in the periphery. All stimuli were presented for 6 cycles of 40 s each. ***A***: Expanding rings continually expanded outward from the fixation point each cycle. ***B***: Rotating wedges revolved 360° clockwise around the fixation point each cycle. ***C***–***D***: Meridian-mapping stimuli. The horizontal and vertical meridians were stimulated using “hourglass” and “bow tie” shaped checkerboard patterns that were alternated every 1/2 cycle. ***E***–***F***: 16° isopter stimuli. A 16° arc subtended the superior or inferior quadrant of the hemifield containing the scotoma. Each arc was presented alternately

with a period of no stimulation every 1/2 cycle. ***G***: Scotoma-mapping stimulus. A contrast-reversing checkerboard pattern was presented to the quadrant of visual space with the scotoma. Patients viewed the stimulus through the right or left eye in alternating 1/2 cycles. The fixation target in the corner also served as a cue as to which eye should be open.

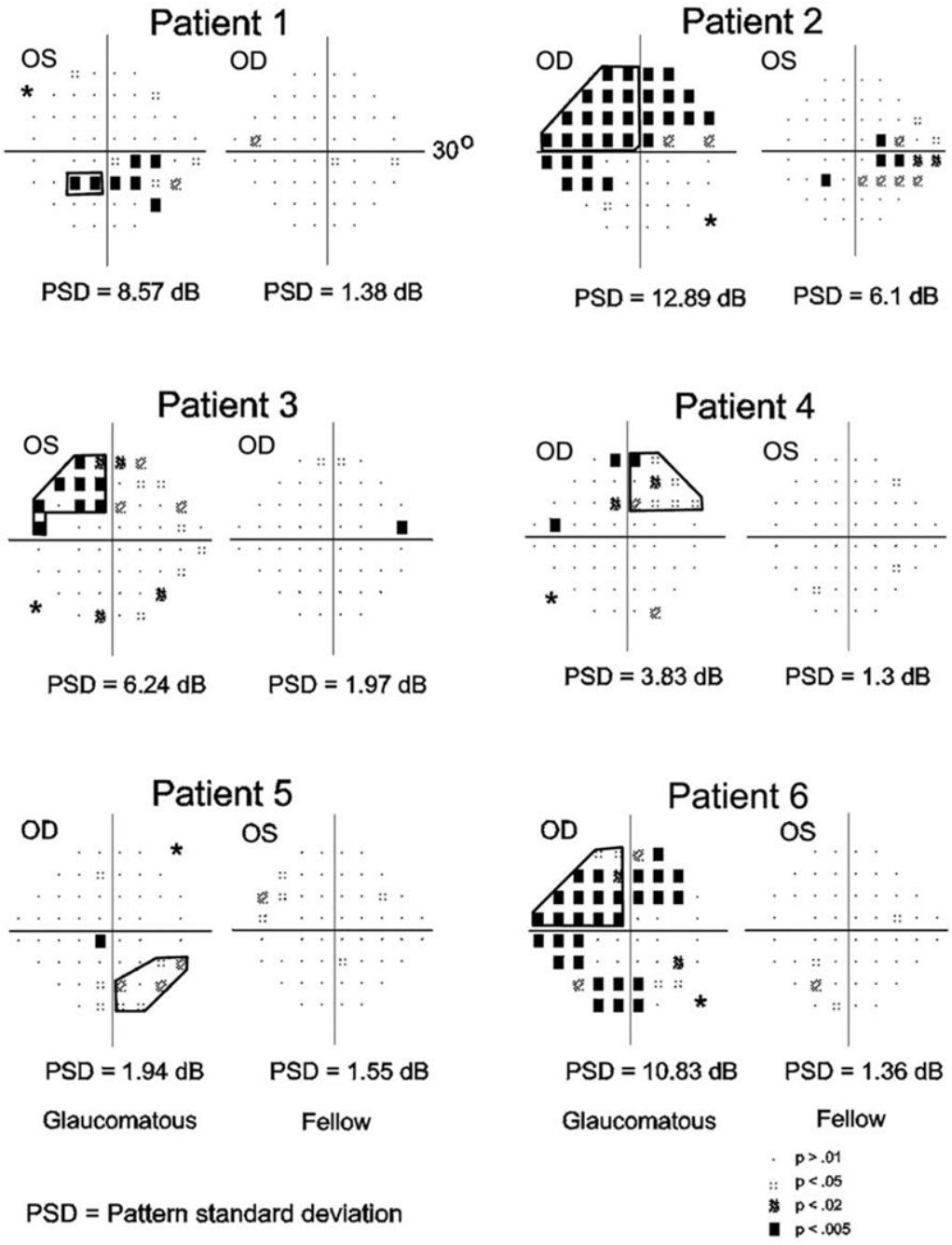

Figure 2. Visual field maps for SAP

Visual field defects were measured using standard automated perimetry. Each panel depicts the pattern deviation plot of each eye for one patient. The deviation from the age-corrected normal values is measured in decibels (dB), and adjusted for any shifts in overall sensitivity. Pattern deviation (PD) symbols indicate the statistical significance of the deviation at each point. Darker symbols represent more significant deviations from the normal thresholds. The experimenter identified a contiguous portion of the visual quadrant with the greatest loss (bold lines). Patients are listed in order from the strongest to the weakest asymmetry as determined by the difference in pattern standard deviation scores (A–E, respectively). Asterisks mark the

quadrant with the least amount of visual loss in the glaucomatous eye, which served as a control. The pattern standard deviation (PSD) global score is also given below each graph.

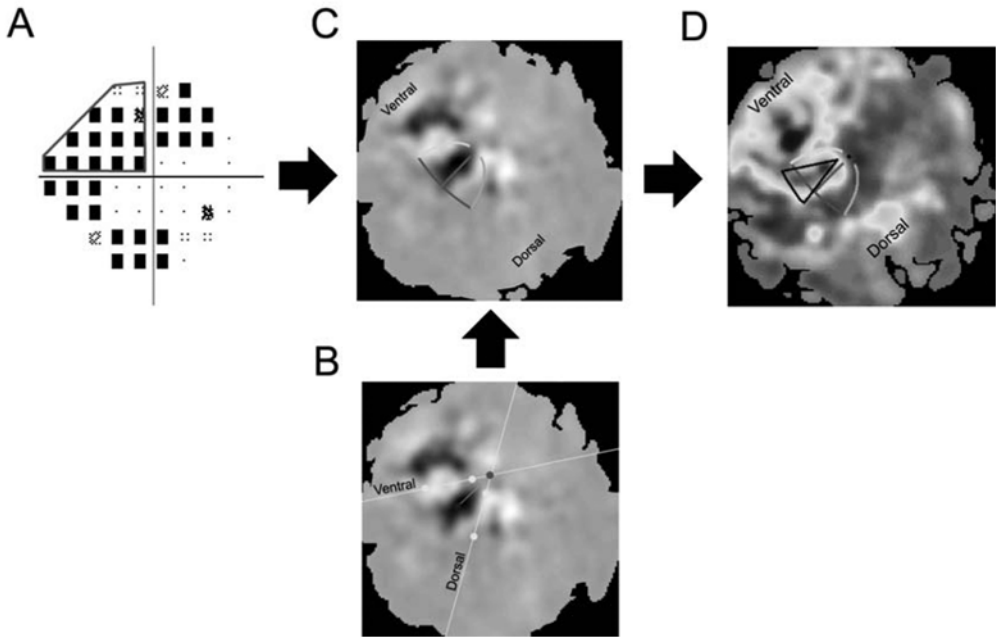

Figure 3. Projecting regions of visual space onto V1

A: Pattern deviation plot of SAP thresholds for the glaucomatous eye of the Patient 6 from Figure 2. A region of visual space in the upper left quadrant was selected with the intent of projecting that region onto the flattened cortex (bold line). ***B***: The initial stages of fitting retinotopic fMRI data. FMRI responses to the meridian mapping stimuli are pictured in gray. White pixels denote responses that were in phase with stimulation of the vertical meridian. Black pixels denote responses that were in phase with stimulation of the horizontal meridian. The experimenter selected two points along the activity patterns for each vertical meridian (yellow dots). The software automatically fit lines (yellow lines) to the points selected and then computed the intersection of those points (red dot), which was assumed to be near the representation of the fovea. The experimenter then selected a point along the activity pattern of the horizontal meridian (blue dot). The software automatically connected the foveal representation with the point along the horizontal meridian (green line). A generic template was positioned and rotated according to the values computed during this stage of the fitting process. ***C***: Template superimposed upon fMRI responses to the meridian-mapping stimuli. After the generic template was generated, each component of the template was fit using an iterative least-squares method (see Figure 3). The template was then used to project regions of visual space onto the flattened cortex. ***D***: The projected scotoma as a ROI. The best-fitting template is presented along with the projected scotoma (black lines) atop the fMRI responses to the scotoma-mapping stimulus (see Figure 5).

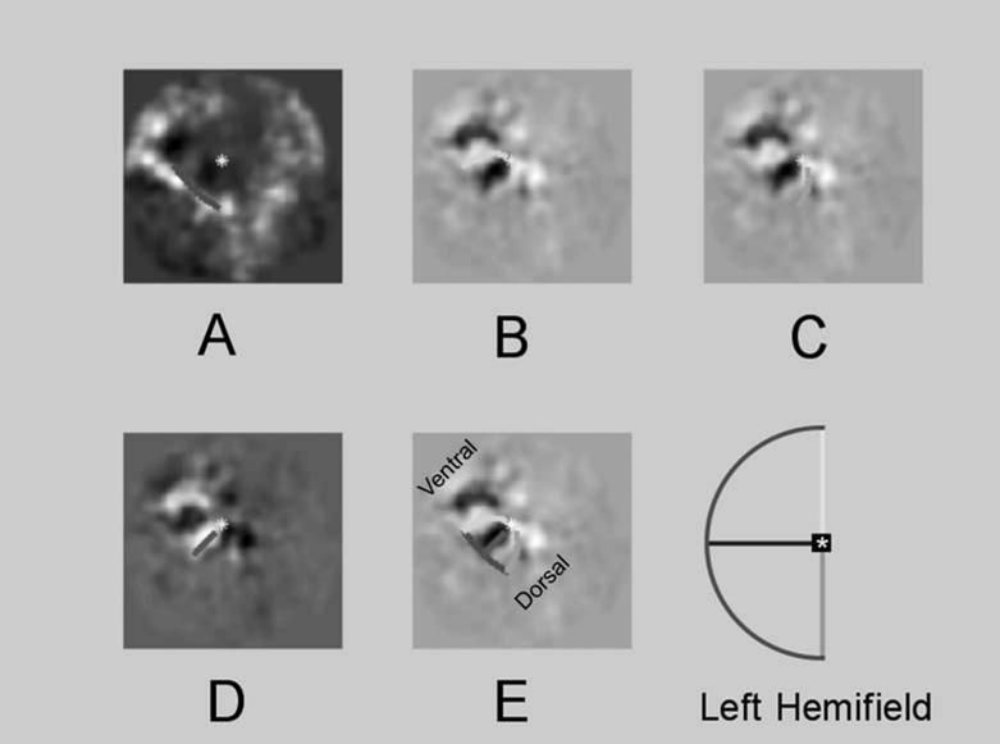

Figure 4. Cortical responses to retinotopic mapping stimuli

Templates derived from conformal mapping techniques were fit to the fMRI activity maps generated by retinotopy stimuli. Grayscale images show BOLD activity maps on the flattened representation of cortex. Templates were fit to maximize the image intensity under the projected curves. Colored lines are components of the best-fitting template. Components are color coded to match the schematic of visual space in the inset. ***A***: Response to the 16º isopter stimuli presented in the left visual hemifield. ***B***: Responses to stimulation of the superior vertical meridian. ***C***: Responses to stimulation of the inferior vertical meridian. ***D***: Responses to stimulation of the horizontal meridian. ***E***: The best-fitting template is superimposed upon responses to the vertical meridian stimulus. Ventral and dorsal regions of occipital cortex are labeled. Note that ***B–D*** depicts three different fits to fMRI responses to the same visual stimulus. The sign of the phase in ***D*** is flipped relative to ***B*** and ***C***.

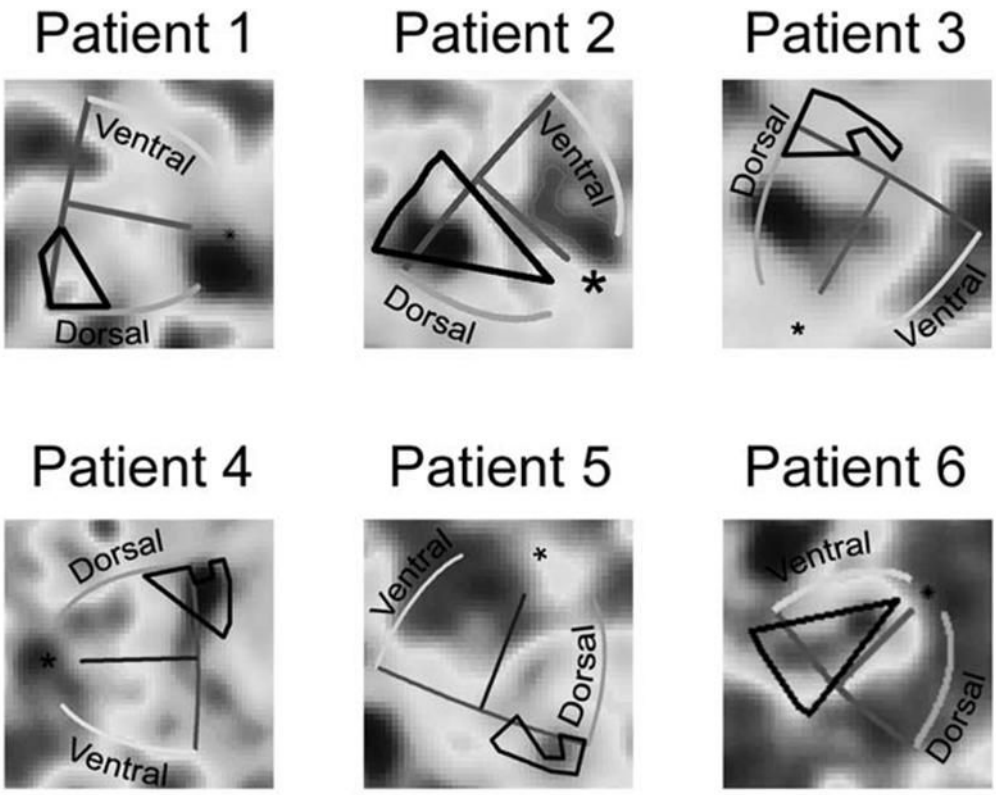

Figure 5. Cortical responses to scotoma-mapping stimuli

Average BOLD response to the scotoma-mapping stimulus is projected onto the flattened representation. Pixel color indicates the phase of the BOLD response relative to the phase of monocular viewing. For patients where greater vision loss occurs in the right eye (Patients 2,4,5 and 6), bluish pixels correspond to voxels that were in phase with viewing through the fellow eye. Yellowish pixels correspond to voxels that were in phase with viewing through the glaucomatous eye. For patients where greater vision loss occurs in the left eye (Patients 1 and 3), yellowish pixels denote voxels that were in phase with viewing through the fellow eye, and bluish pixels represent voxels in phase with the viewing through the glaucomatous eye. The best-fitting template (colored lines) and the ROI (black line) are superimposed on the data. Voxels within the ROI indicate a greater BOLD response when viewing through the fellow eye.

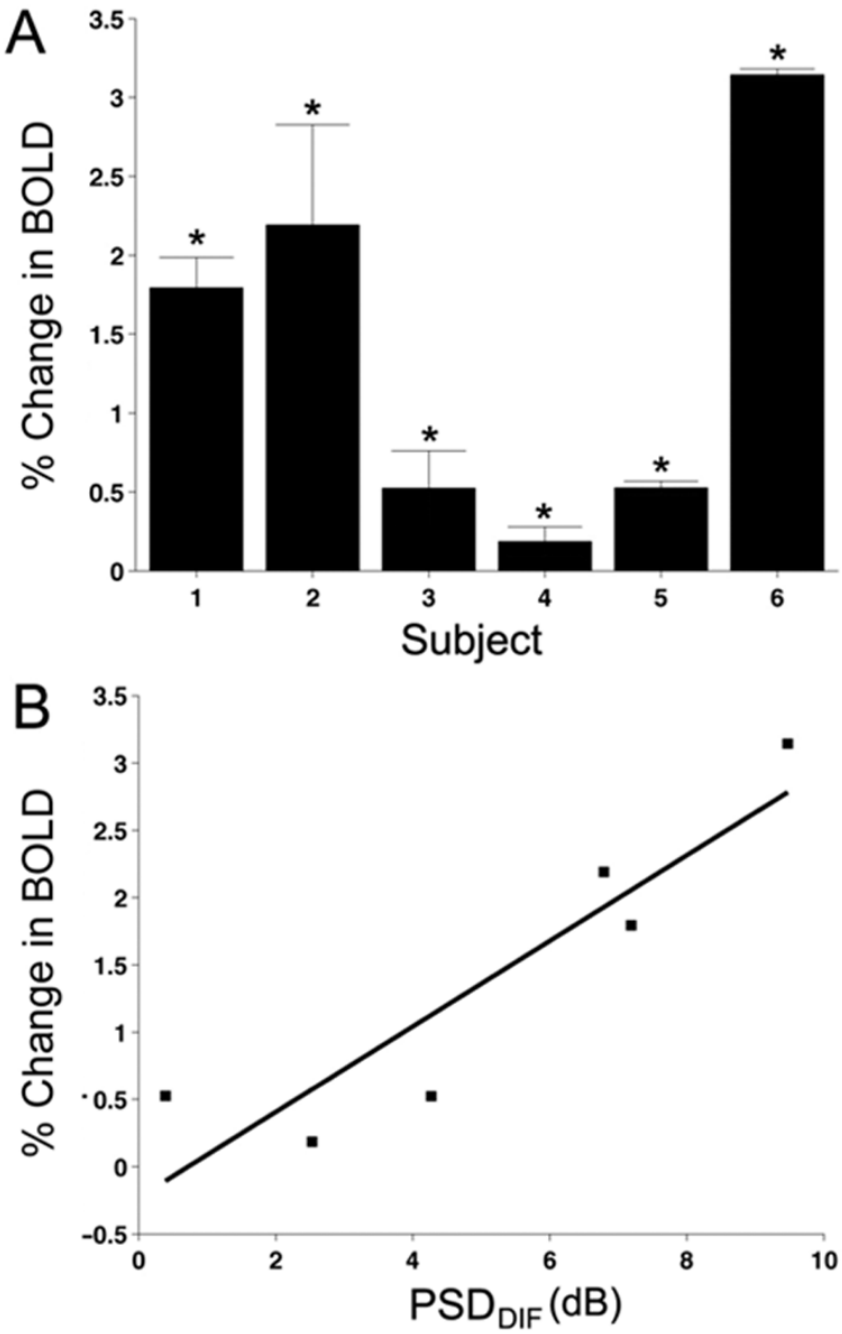

Figure 6. Cortical responses to scotoma-mapping stimuli for all patients

A: FMRI responses are plotted as the percent change in BOLD amplitude for all six patients. The percent change in BOLD amplitude for each patient was averaged across eight scans. The sign of the fMRI response was multiplied by 1 or −1 depending on which eye was affected for each patient. Positive numbers indicate viewing through the fellow eye evokes a larger response than viewing through the glaucomatous eye. All six patients demonstrated significantly positive change in BOLD amplitudes. ***B***: Comparison between SAP visual fields and cortical responses. FMRI responses to the scotoma-mapping stimulus were compared to the PSD scores from visual field testing. The PSD from the fellow eye was subtracted from the glaucomatous

eye to yield a difference score for each patient (PSD_{DIF}). PSD_{DIF} scores for SAP were correlated with the difference in fMRI for viewing through the fellow vs. glaucomatous eyes.

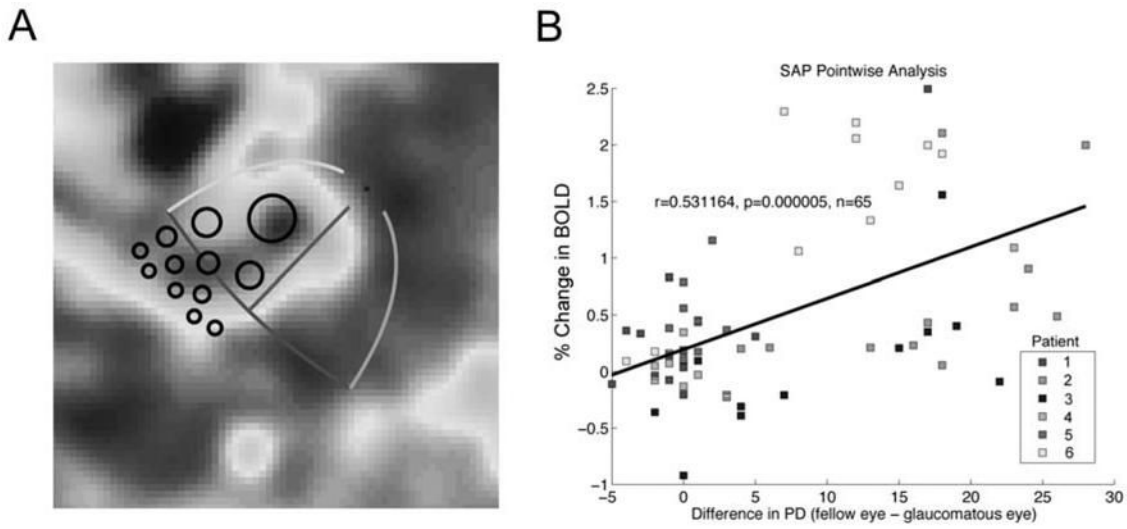

Figure 7. Pointwise comparison of fMRI data and visual thresholds

A: ROIs for the pointwise comparison. Twelve individual ROIs for each patient were derived from twelve test locations from the automated perimetry. For each test location, a 6°-diameter region of visual space was projected onto the flattened representation of cortex using the best-fitting template for each patient. The amplitude of the BOLD signal for voxels within the ROI was compared to corresponding points from the automated perimetry. ***B***: Pointwise correlation between fMRI data and SAP. The difference between PD values for the glaucomatous and fellow eyes were computed for 12 test locations within the damaged visual quadrant. These difference scores were compared to the percent change in BOLD amplitude of the voxels within the corresponding ROI. Each point represents a comparison between the change in BOLD amplitude within a single ROI to the PD difference score for a single test location in one patient. There was a pointwise correlation between the fMRI data and SAP data. The color of each point indicates the responses from each patient.

Table 1

Summary of patient data

PATIENT		**1**		**2**		**3**		**4**		**5**		**6**	
AGE		58		76		68		77		74		63	
SEX		Male		Female		Female		Female		Male		Male	
EYE *		OD_F	OS_G	OD_G	OS_F	OD_F	OS_G	OD_G	OS_F	OD_G	OS_F	OD_G	OS_F
ACUITY$_G$		20/20	20/25	20/40	20/20	20/30	20/20	20/30	20/30	20/20	20/20	20/30	20/20
IOP$_G$		17	16	14	14	15	14	14	15	18	18	12	18
R_x	***Sph.***	1.25	3.0	−1.75	0.25	−6.25	−6.5	1.5	1.75	−1.5	−0.75	1.5	0.75
	Cyl.	-	0.75	0.25	0.5	-	-	1.25	0.75	-	0.75	0.75	-
SURGERY †		TP, L	TP	TP	TP	-	TP	CE	CE	CE	-	TP, TE, CE	-
SAP ‡	**MD** § **(dB)**	−0.3	−6.23	−17.04	−4.78	−4.91	−8.69	−6.43	−2.77	−2.41	−0.66	−14.51	0.80
	PSD(dB)	1.38	8.57	12.89	6.10	1.97	6.24	3.83	1.30	1.94	1.55	10.83	1.36
BOLD P-VALUE		<0.0001		0.005		0.03		0.044		<0.0001		<0.0001	

* G = Glaucomatous eye, F = Fellow eye

† TE = Trabeculectomy, TP = Trabeculoplasty, CE = Cataract extraction with intraocular lens implant, L = Lasic

‡ SAP = Standard automated perimetry

§ MD = Mean deviation scores, PSD = Pattern standard deviations scores

P-values indicate the significance of the BOLD signal for voxels within the cortical representation of the scotoma